http://dx.doi.org/10.5012/bkcs.2014.35.3.908

Fabrication of Micrograting and their IR Diffraction Spectra†

In Cheol Kim, Eunwoo Choi,‡ Seong Kyu Kim,‡,* Young Il Kang,§ Taeseong Kim,# Hyo-Wook Bae,# and Do-Hyun Park#

National Institute for Nanomaterials Technology, Pohang 790-784, Korea
*‡Department of Chemistry, Sungkyunkwan University, Suwon 440-746, Korea. *E-mail: skkim@skku.edu*
§The 5th R&D Institute - 2, Agency for Defense Development, Daejeon 305-600, Korea
#MOORI Technologies Co., Yongin 449-863, Korea
Received October 8, 2013, Accepted October 11, 2013

Microgratings whose diffracted field at a fixed angle generate IR spectra of SF_6 or NH_3 were fabricated by MEMS techniques for the purpose of IR correlation spectroscopy. Each micrograting was composed of 1441 reflecting lines in the area of 19.2 × 19.2 mm^2. The depth profile of the line elements was determined with a gradient searching method that was described in our previous publication (*J. Mod. Opt.* **2013**, *60*, 324-330), and was discretized into 16 levels between 0 and 6.90 μm. The diffraction field from a given depth profile was calculated with Fraunhofer equation. The fabricated microgratings showed errors in the depth and the width within acceptable ranges. As the result, the diffracted IR spectrum of each micrograting matched well with its target reference spectrum within spectral resolution of our optical setup.

Key Words : Micrograting, Gradient search, MEMS, IR spectrum, Fraunhofer diffraction

Introduction

The micrograting is an optical element which diffracts light with desired spectral intensity. One of its applications is the correlation spectroscopy,[1-3] in which a micrograting generates a target spectrum whose correlation with a sample spectrum can identify the target molecule in the sample mixture. Microgratings may take on a fixed pattern to be used for a specific target or a programmed variable pattern to generate multiple target spectra. In either way, modern MEMS technology is a key.

When a broad band light is incident normally onto a micrograting, the diffracted field $U(\lambda, \theta)$, detected at a specific angle θ, can be described by Fraunhofer equation,[4]

$$U(\lambda, \theta) = \frac{C}{\lambda} \int_{-\infty}^{\infty} \exp\left\{-i\frac{4\pi d(x)}{\lambda}\right\} \exp\left(-i\frac{2\pi x \sin\theta}{\lambda}\right) dx \quad (1)$$

where C is a constant, x is the grating axis, and $d(x)$ is the depth pattern of the micrograting. In case the micrograting is made of M reflecting line elements of equal width Δ and depth profile $\{d_m\}$, where $m = 1, \ldots, M$, the depth pattern can be expressed as[5,6]

$$d(x) = \sum_{m=1}^{M} d_m rect\left(\frac{x - m\Delta + \Delta/2}{\Delta}\right) \quad (2)$$

where *rect* represents the rectangular function. The depth profile $\{d_m\}$ can be obtained by minimizing the difference between the calculated spectral intensity $|U(\lambda, \theta)|^2$ and the target spectral intensity.

In our recent publication,[5] we demonstrated that a gradient searching Davidon-Fletcher-Powell (DFP) algorithm[6-8] is very effective in optimizing the depth profile $\{d_m\}$ to retrieve IR spectra of gases. The IR spectra of SF_6, NH_3, SO_2 and ethylene at the diffraction angle $\theta = 15^o$ were successfully retrieved in the spectral range of 725-1450 cm^{-1} using 1126 parallel lines in the overall size of 1.5 cm.

Once the depth profile is optimized, extra analysis would be possible with the Fraunhofer equations (By "the Fraunhofer equations" authors mean Eq. (1) and accompanying equations (*e.g.* Eq. (2)) to calculate diffraction field under a given depth profile. See reference 5). First, the diffraction efficiency can be calculated by dividing $|U(\lambda, \theta)|^2$ by the reflection intensity $|U(\lambda, 0)|^2$ with all d_m's set to 0. The analysis in our recent publication[5] showed that the optimized depth profile with the DFP algorithm provides superior diffraction efficiency as well as the spectrum matching to other methods such as phase retrieval algorithm.[2,3,7] Second, by introducing variations to the width or the depth of individual lines, effects of the width error or the depth error during the MEMS fabrication process can be predicted.

While the microgratings were successfully designed with the predictable error effects, it is our concern how accurately the microgratings can be made to generate target spectra. For this task, microgratings, designed with the DFP algorithm for target spectra of SF_6 and NH_3, were fabricated by MEMS techniques and their diffraction spectra were obtained in an optical setup.

Experimental

Sample Preparation. Three different kinds of optical elements, which can be interchanged with little mis-alignment in a micrograting holder of our optical setup, were prepared.

†This paper is to commemorate Professor Myung Soo Kim's honourable retirement.

The first and most important kind is the target microgratings for SF_6 and NH_3. The active area of each micrograting was 19.2×19.2 mm^2, composed of 1441 reflecting line elements (thereby $\Delta = 13.323$ mm) whose depths were discretized into 16 levels.

Sixteen replicas of a target micrograting were inscribed on a six-inch silicon wafer. Each target micrograting was patterned in a sequence of four step etchings using four masks produced by photolithography. The first and the second etching steps were done by an ICP etcher (DMS, Igeminus-2000) for the depths of 0.46 μm and 0.92 μm, respectively. The third and the fourth etching steps were done by a deep etcher (STS, Multiplex Lite ASE-SR) for the depths of 1.84 μm and 3.68 μm, respectively. For each etching process, each mask was imprinted with a photoresist track system (TEL, Mark 7) and a stepper system (NIKON, NSR 2205 i10c). After the four etchings, Ti/Au thin layer was coated with the thickness of 0.02 μm/0.3 μm. After the final Ti/Au coating, the depths and the widths of 100 line elements from a selected micrograting were measured with a 3D-profiler (VEECO, NT1100) and a high resolution FE-SEM (JEOL, JSM-7401F), respectively.

The second kind is a standard grating which diffracts a 1000 cm^{-1} peak at $\theta = 15^o$. This grating has a square wave pattern with the periodicity of 38.637 μm and is used to optimize and characterize our optical setup. The diffraction efficiency, calculated by the Fraunhofer equations, is highest (40%) when the height of the square wave is 2.5 μm. The standard grating can be fabricated in a single process of photolithography, etching, and Ti/Au coating. The third kind is a 7.5^o wedge mirror which can guide the 15^o beam under visible condition. This wedge mirror is useful not only for initial alignment of the optical setup but also for obtaining diffraction efficiencies of microgratings.

Optical Setup. Figure 1 shows the optical setup to obtain the diffraction spectra of microgratings. An IR illuminator (NEWPORT, Apex, 24 W SiC element) coupled with a monochromator (NEWPORT, Cornerstone 260, f = 25 cm) provides the light source. In the monochromator, a grating (75 lines/mm, blazed at 7 μm) is used to provide a monochromatic IR beam and it is switchable to a mirror when beam alignment is needed or when the correlation spectroscopy is exercised. After a long pass filter (EDMUND, cut-on wavelength at 7.3 μm), the monochromator output is collimated by a 90^o off-axis parabolic gold mirror (f = 203 mm) and is incident normally onto a sample (micrograting, standard grating, or wedge mirror) to be tested. The diffraction beam at $\theta = 15^o$ is then focused by a 90^o off-axis parabolic gold mirror (f = 150 mm) onto a manual slit in front of a liquid nitrogen cooled mercury-cadmium-telluride (MCT) detector (INFRARED ASSOCIATES). The MCT signal goes through a preamplifier (INFRARED SYSTEMS DEVELOPMENT, MCT-1000) and is fed into a lock-in-amplifier (SIGNAL RECOVERY, 7280). The monochromator control and the lock-in-amplifier signal reading are interfaced synchronously with GBIP (National Instrument) and Lab View program. The parabolic gold mirror in front of the MCP detector is mounted on an *xyz* translation stage, in which one axis (*y*-axis, see Figure 1) is controlled by a stepper (NEWPORT, LTA-HS and ESP301).

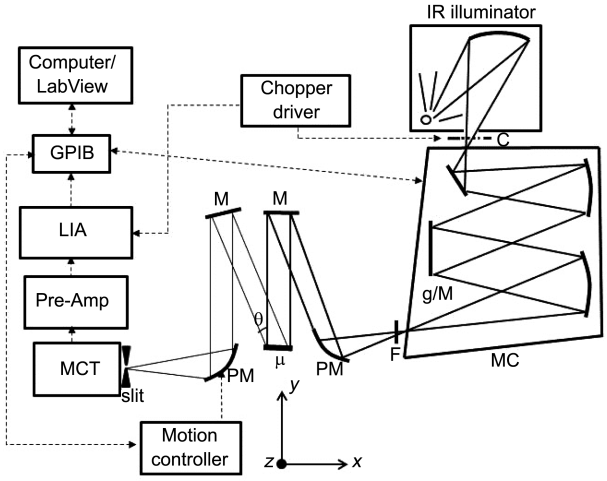

Figure 1. Layout of the optical setup for testing micrograting; C: chopper, MC: monochromator, g/M: interchangeable grating and mirror, M: mirror, PM: 90^o off-axis parabolic mirror, μ: micrograting, MCT: mercury-cadminum-telluride detector, LIA: lock-in-amplifier, GPIB: general purpose interface bus.

Results

Micrograting Profile. Examples of the depth profile and the width profile measurements are shown in Figure 2. The depth profile in Figure 2(a), provided by a 3D-profiler, shows artifacts in the vicinity of line element edges due to interference in the 3D-profiler. Therefore, the depth data were obtained in the middle of each line element. By comparing them with the FE-SEM measurements (Figure 2(b)), the 3D-profiler depth measurement was proved to have the accuracy within 0.1 μm.

Four replica microgratings, located in the central part of each patterned wafer, were investigated with the 3D-profiler. The depths of 100 line elements in each selected micrograting were compared with the designed depth profile data to find the error distribution. The results are summarized in Table 1.

For the FE-SEM measurements, it is inevitable to cut a sample for sectional view, and the cut sample could not be used for spectrum measurement. However, after several measurements, we were convinced that the width error distribution is not so much different from sample to sample since it comes mainly from the mask alignment error which is usually same within a wafer. In contrast, the depth error comes mainly from the etching rate variation over a wafer area. Therefore, while the depth error needs be measured individually for each micrograting, the single measurement with FE-SEM may sufficiently represent the width error characteristics of all microgratings.

Figure 2(b) is an example of FE-SEM image for the cross-sectional view. More often than not, a tiny narrow wall

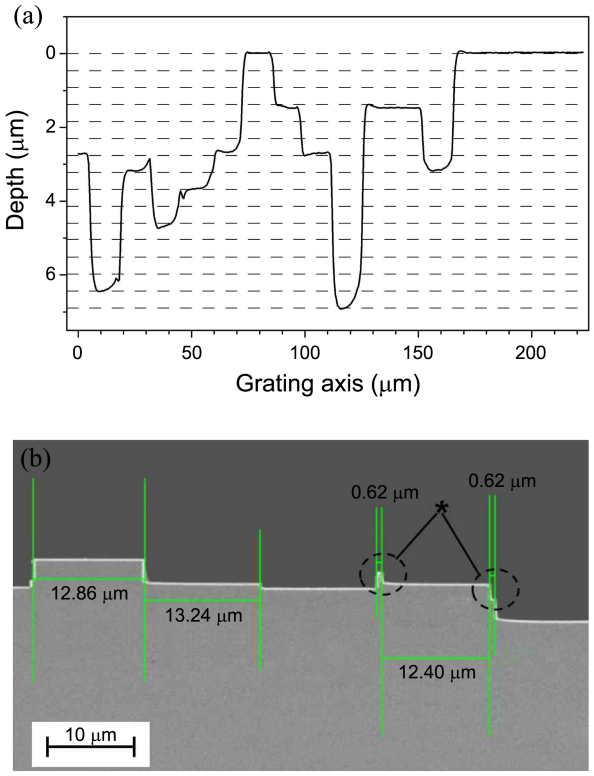

Figure 2. Examples of the depth profile measurement by 3D-profiler (a) and the width profile measurement by FE-SEM (b). In the 3D-profiler plot, the 16 levels are indicated with broken straight lines.

Table 1. The depth error and the width error from 3D profiler and FE-SEM measurements. σ: the standard deviation assuming Gaussian distribution

Micrograting sample		Depth error		Width error	
		Mean (μm)	σ (μm)	Mean (μm)	σ (μm)
SF_6	No. 1	0.18	0.18		
	No. 2	0.24	0.25		
	No. 3	0.22	0.22		
	No. 4	0.17	0.18		
NH_3	No. 1	0.28	0.26		
	No. 2	0.32	0.32		
	No. 3	0.41	0.40		
	No. 4	0.37	0.32		
	No. 5			-0.05	0.46

followed by a cut step (the ones indicated with black circles in Figure 2(b)) is seen at edges of line elements. Such defects, produced by possible mask mis-alignment, are certainly undesirable since they may scatter light. However, we did not attempt to remove them by additional oxidation and wet etching since the extra job shall induce further width variations and the defects are found in less than 2% of the line elements. The width error distribution is also summarized in Table 1.

Diffraction Spectra. In order to resolve the diffraction spectra better, the slits at the detector and the monochromator must be as narrow as possible. In contrast, the signal intensity is lower at narrower slits. Therefore, we had to determine optimal slit sizes which compromise the spectral resolution and the signal intensity. It was done by measuring focal sizes at the detector slit and investigating the signal intensity variation with monochromator slit sizes. Afterwards, the spectra we report here were obtained with 100 μm, 200 μm, 300 μm for the slit sizes at the detector, at the monochromator exit, and at the monochromator entrance, respectively.

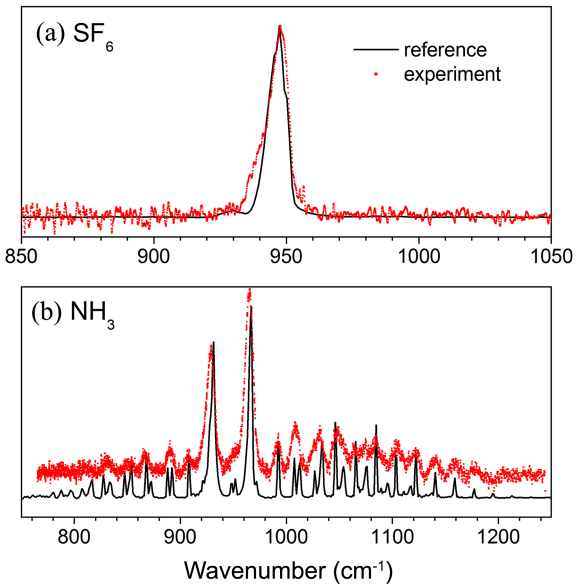

Figure 3. Diffraction spectra from SF_6 (a) and NH_3 (b) micrograting. Solid line curves are from reference spectra and dotted curves are from measurements. In each measured spectrum, the raw spectrum is divided by the spectrum of incident light. In (b), the measured NH_3 spectrum is shifted vertically for better distinction with the reference spectra. The measured spectra are from No. 1 samples in Table 1.

When the diffraction spectrum from the standard grating was obtained, a single peak at 1000 cm^{-1} was observed with the bandwidth of 3.6 cm^{-1} in FWHM (spectrum not shown). This should correspond to the upper limit of the bandwidth of the optical setup.

The diffraction spectra of SF_6 and NH_3 microgratings are shown in Figure 3, overlapped with the corresponding reference spectra from database library of MIDAC Co. The reference spectrum of SF_6 shows a single band at 947 cm^{-1}, assigned to T_{1u} vibration. The band takes on asymmetric shoulders due to unresolvable rotational structures (rotational constant B ~0.1 cm^{-1}). The measured spectrum matches well with the reference except the low intensity features.

In contrast to the simple SF_6 spectrum, the NH_3 reference spectrum is very complicated. It consists of a pair of vibrational peaks at 931.7 cm^{-1} and 968.3 cm^{-1}, due to Fermi resonance splitting of an inversion vibration[9,10] and overlap of their rotational lines (rotational constant B ~9.98 cm^{-1}). Considering the complex reference spectrum, the measured diffraction spectrum is acceptable; it shows good matches in the strong vibrational peaks and many resolvable rotational

lines, while some small or closely-spaced rotational lines were not resolved.

In fact, there were a few experimental difficulties in obtaining the NH_3 spectrum in better resolution. First, the diffraction efficiency of the NH_3 is three times lower than that of SF_6. Second, the sensitivity of the optical setup, resulted from incident light spectrum, the monochomator grating efficiency, the long pass filter spectrum, and the MCT detector response, drops rather rapidly as the wavenumber goes below 1000 cm^{-1}. Third, there was small interference due to electronic background noise which we were not able to remove completely. For these reasons, we were not able to close the slits further for better resolution. The FWHM of the two vibrational peaks are 8.5 cm^{-1}, which is broader than 3.6 cm^{-1} measured with the standard grating under the same slit condition. The difference may be attributable to that the reference NH_3 spectrum itself has the peak bandwidth of 3.5 cm^{-1} and that the width error in the MEMS fabrication process may induce additional broadening.

Diffraction efficiencies of the standard grating and the two kinds of microgratings were measured by comparing diffraction intensities at their peaks with signal intensities when they were replaced by a wedge mirror under the same experimental condition. They were very close to the diffraction efficiency calculated with the Fraunhofer equations (*i.e.* 40% for the standard, 5.9% for SF_6, and 1.9% for NH_3).

Discussion

In correlation spectroscopy, shifting target spectrum from sample spectrum is necessary. This can be done easily in our optical setup by translating the parabolic focusing mirror along *y*-axis in Figure 1. As this action is same as varying the detection angle θ, we calculated a series of spectra at variable θ using the Fraunhofer equations; this gives the angular dispersion of the micrograting $d\theta/d\lambda$. The calculation shows a constant angular dispersion, $d\theta/d\lambda = 1.46 \times 10^{-3}$ degree/nm, when θ is varied between 14.0° and 16.0°. Then, the linear dispersion $dy/d\lambda$ at the detector slit, which must equal the focal length of the parabolic mirror times $d\theta/d\lambda$, is calculated to 3.82 μm/nm. We were able to verify this relation by obtaining a series of shifted spectra at variable *y* (spectra not shown). The fact that the linear shift of spectra is guaranteed with the parabolic mirror system would be advantageous over focusing with a lens or a spherical concave mirror.

How the depth and the width errors shown in Table 1 might have affected the diffraction spectra is worth to discuss. The mean value of the depth error (that is, about 0.2 μm for SF_6 or about 0.3 μm for NH_3) means that all line elements are translated equally by that much in the depth axis. Therefore, it would not influence the spectrum since relative phase of each line element is invariant. The effect of standard deviation in the depth error was discussed in our previous publication.[5] A wider distribution in depth error generates a noisier spectrum while maintaining main features in the diffraction spectrum.

Effects of the width error needs more elaborate consideration. The mean value of the width error is −0.05 μm. Although this error is small, considering the precision of photolithographic preparation of masks, the spectrum may have been affected. For this purpose, we calculated the diffraction spectrum of NH_3 micrograting with the reduced width using the Fraunhofer equations. The calculated spectrum showed that all peaks shifted equally by −40 nm without changing spectral shape. The shift corresponds to about +4 cm^{-1} in wavenumbers. This kind of shift is always ignored during the spectrum collection since the horizontal position (*y*-axis) of the parabolic focusing mirror is adjusted slightly to match one strong peak wavelength to the reference value. This is necessary since it is not possible to know the exact diffraction angle when the spectrum is collected. Considering the angular dispersion $d\theta/d\lambda = 1.46 \times 10^{-3}$ degree/nm, the 40 nm shift induced by −0.05 μm width error implies that the spectra in Figure 3 were indeed obtained at θ = 14.6°.

The effect of the width error distribution was discussed in our previous publication.[5] We demonstrated that a small distribution in width error shall increase the bandwidth but a wider distribution than about 0.04Δ in standard deviation shall distort the spectral shape. 0.04Δ corresponds 0.53 μm in our microgratings. This limit is not trivial to meet since conventional mask alignment error in a single step etching is about 0.3 μm and this error tends to be accumulated in multiple etching steps. Nevertheless, we were able to meet this limit with careful alignment checking processes.

As we are interested in whether our optical system is effectively set up to resolve the diffraction spectrum, the diffraction limited focal diameter D at the detector slit is calculated,[11,12]

$$D = 0.45 \times 2(2\ln 2)^{1/2} \times (F\#) \times \lambda$$
$$= 1.06 \times (7.8) \times (10\ \mu m) = 83\ \mu m,$$

where D is in FWHM of a Gaussian shaped focal spot and F# is the F number of the focusing optics. To be compared, we measured the focal diameter at the detector slit to 130 μm under the monochromator slit condition of this work. Therefore, the experimental focal size is larger by 1.6 times than the theoretical one. Two factors are thought to be responsible for the focal size difference. First, since the monochromator slit could not be closed completely, the incident beam is slightly out of collimation. Second, the parabolic mirror focusing is sensitive to input beam direction. Although the parabolic mirror focusing, in free of aberations, may focus light more closely to its diffraction limit than focusing with a convex lens or a spherical concave mirror, a slight misdirection of incident light results in rather big deviation from the diffraction limit.[13]

The value of linear dispersion ($dy/d\lambda$ = 3.82 μm/nm) and the experimentally determined focal diameter (130 μm) can be used to calculate the bandwidth when a known size of slit is placed at the detector. Our calculation results in 3.8 cm^{-1} when 100 μm slit is placed, in good agreement with the measured bandwidth.

Reducing the bandwidth of optical setup further cannot be

achieved by selecting different focal length since the linear dispersion and the focal size depend on the focal length in the same way. The other plausible way for the bandwidth reduction is to increase the micrograting size. The micrograting of larger size reduces the F number and the focal size while the linear dispersion is unaffected. However, we have not obtained such a result when we compared the focal sizes and bandwidths of two different sizes of standard gratings, 15×15 mm^2 and 19.2×19.2 mm^2; they gave virtually same focal sizes and bandwidths. Although the larger size gratings are to give reduced focal sizes theoretically, the effect is obscured by practical problems in using the parabolic mirror focusing. The two considerations imply that trying to improve spectral resolution by changing optical setup would be unsuccessful. Therefore, the only way to improve the spectral resolution is to increase the detection sensitivity so that narrower slits can be adopted. In this respect, we believe that the spectra in Figure 3 are practically close to the best result which can be obtained using current stage of instruments.

Conclusion

In our previous work, we developed a gradient searching Davidon-Fletcher-Powell algorithm to design micrograting patterns to retrieve diffraction spectra of target gases. Further development is achieved in this work; their microgratings can be fabricated from reliable MEMS process to give good enough diffraction spectra for correlation spectroscopy. The fabrication errors are so small that the diffracted spectrum is little affected.

The target gases in this study, SF_6 and NH_3, exhibit two extreme spectra in the frequency range of interest: one is the most simple and the other is the most complicated. Therefore, the correlation spectroscopy for the two gases may provide standard information for other target gases. As both gases can be treated in laboratory with little hazard precaution and the optical setup of this study can be used directly for the correlation spectroscopy, we expect to report results soon from the correlation experiments.

Acknowledgments. This work was carried out with a fund for Chemical and Biological Detection Research Center.

References

1. Goody, R. *J. Opt. Soc. Am*. **1968**, *58*, 900.
2. Sinclair, M. B.; Butler, M. A.; Ricco, A. J.; Senturia, S. D. *Appl. Opt*. **1997**, *36*, 3342.
3. Sinclair, M. B.; Butler, M. A.; Kravitz, S. H.; Zubrzycki, W. J.; Ricco, A. J. *Opt. Lett*. **1997**, *22*, 1036.
4. Goodman, J. W. *Introduction to Fourier Optics*, 2nd ed.; McGraw-Hill: New York, 1996; Ch. 4.
5. Kim, T.; Kim, S. K.; Kim, I. C.; Bae, H.-W.; Park, D.-H. *J. Mod. Opt.* **2013**, *60*, 324.
6. Zhou, G.; Tay, F. E. H.; Chau, F. S. *Opt. Express* **2003**, *11*, 1392.
7. Sagberg, H.; Lacolle, M.; Johansen, I.-R.; Løvhaugen, O.; Belikov, R.; Solgaard, O.; Sudbø, A. S. *IEEE J. Selected Topics in Quant. Elect*. **2004**, *10*, 604.
8. Wolfe, M. A. *Numerical Methods for Unconstrained Optimization: an introduction*; Van Nostrand Reinhold Co.: New York, 1978; Ch. 6.
9. Hollas, J. M. *High Resolution Spectroscopy*; Butterworh & Co.: London, 1982; Ch. 5.
10. Wood, D. L.; Bell, E. E.; Nielsen, H. H. *Proc. Natl. Aca. Sci. USA* **1950**, *36*, 497.
11. Hecht, E.; Zajac, A. *Optics*; Addison-Wesley Publ. Co.: 1979; Ch. 10.
12. Meinhart, C. D.; Wereley, S. T. *Meas. Sci. Tech.* **2003**, *14*, 1047.
13. Liu, X.; Lu, Z.; Wang, X.; Jiang, Z.; Li, Y. *Optoelectronics and Microelectronics Technology (AISOMT), 2011 Academic International Symposium on IEEE*, 2011; p 116.